UDK 669.715:621.78
Professional article/Strokovni članek

ISSN 1580-2949
MTAEC9, 48(1)141(2014)

THE EFFECT OF HEAT TREATMENTS ON THE SOLID-PARTICLE EROSION BEHAVIOR OF THE ALUMINUM ALLOY AA2014

VPLIV TOPLOTNE OBDELAVE ZLITINE AA2014 NA VEDENJE PRI EROZIJI S TRDNIMI DELCI

Sedat Karabay
Mechanical Engineering Department of Engineering Faculty of Kocaeli University, Kocaeli, Turkey
sedatkarabay58@gmail.com

Prejem rokopisa – received: 2013-03-18; sprejem za objavo – accepted for publication: 2013-05-20

In this study the solid-particle erosion behaviour of solutionised, artificially aged (T6) and annealed specimens prepared from an extruded aluminium alloy AA2014 was investigated and an intercomparison was made. The samples were eroded in specially designed, solid-particle erosion test equipment at a 45° impingement angle and 75 m/s impingement velocity by using 180-mesh garnet erodent particles. Microstructures of the solutionised, artificially aged and annealed samples from the AA2014 were obtained using a light microscope. Moreover, the Vickers hardness of the samples exposed to different heat treatments was measured in order to evaluate the erosion rates with respect to the ductility changes in the material. Additionally, the surface morphology images of the samples were taken before and after the erosion test using a scanning electron microscope (SEM). The results showed that the heat treatments dramatically affected the erosion rates of the samples. However, artificially aged samples caused decrease reduction of the erosion resistance of the AA2014 aluminium alloy. The solutionised alloy showed the best erosion resistance compared to the precipitation hardening (T6) and annealed samples. The effects of the microstructures and the hardness on the erosion behaviour of the different heat-treated specimens were discussed. Finally, SEM images of the samples were analyzed in detailed and the erosion mechanism occurring on the surfaces of the samples was discussed.

Keywords: AA2014, impingement angle, erosive loss, erodent particle, flake, craters

V tej študiji je bila izvršena preiskava in primerjava vzorcev, izdelanih iz ekstrudirane aluminijeve zlitine AA2014, raztopno žarjenih, umetno staranih (T6) in mehko žarjenih, na vedenje pri eroziji s trdnimi delci. Vzorci so bili erodirani v posebno konstruirani napravi za preizkušanje erozije s trdnimi delci pri naklonu udarca 45° in hitrosti udarca 75 m/s, pri uporabi delcev granulacije 180. S svetlobno mikroskopijo je bila pregledana mikrostruktura raztopno žarjenih, umetno staranih in popuščanih vzorcev iz AA2014. Izmerjena je bila tudi trdota po Vickersu vzorcev, izpostavljenih različnim toplotnim obdelavam, da bi opredelili hitrost erozije glede na spremembe plastičnosti materiala. Z vrstičnim elektronskim mikroskopom (SEM) smo dodatno napravili tudi posnetke morfologije površine vzorcev pred preizkusom erozije in po njem. Rezultati so pokazali, da toplotna obdelava vzorcev močno vpliva na hitrost erozije. Vendar pa je umetno staranje vzorcev povzročilo zmanjšanje odpornosti proti eroziji zlitine AA2014. Raztopno žarjena zlitina je pokazala najboljšo odpornost proti eroziji v primerjavi z izločevalno utrjenimi (T6) in mehko žarjenimi vzorci. Komentiran je tudi vpliv mikrostrukture in trdote različno toplotno obdelanih vzorcev na vedenje pri eroziji. SEM-posnetki vzorcev so detajlno analizirani in opisani so mehanizmi erozije, ki so se pojavili na površini.

Ključne besede: AA2014, naklon udarca, izgube pri eroziji, erozijski delec, luske, kraterji

1 INTRODUCTION

Applications for the 2*xxx* series alloys include the internal and external structures of aircraft, the structural beams of heavy dump and tank trucks and trailer trucks, the fuel tanks and booster rockets of the space shuttle and internal railroad car structural members. AA2014 is the most popular type of 2xxx series group for producing mechanical constructions. It is obvious that all of these parts are exposed to various types of particle erosion following the completion of the construction.[1] Erosion is described as the progressive loss of original material from a solid surface due to a mechanical interaction between the surface and a fluid, which may be a multi-component fluid or impinging solid or liquid particles. It is common that the materials used in pipes, bends and tanks, etc., in industries like chemical, cement, mining and mineral processing and thermal power plants encounter erosion-related problems. Pulveriser mill components, multiple port outlet, orifice, PF (packet filter) bends, elbow, burner assembly, pressure parts, ID (induced draft) fan blade and coal ash slurry pipes are the main components affected by erosion in thermal power stations. There has always been an attempt to reduce the material loss due to erosion as it incurs a huge loss of the material. In the past few decades, researchers have focused on the study of material loss in order to conserve both material and energy.[2] A wide variety of methods were adopted to protect materials from the problems of wear, including the use of efficient materials,[3] processing techniques,[4] surface treatments[5,6] of the exposed components and the use of engineering skills leading to a reduced impact of wear on the material, such as an appropriate impingement angle of the erodent and the velocity of the slurry. The methodology to be followed for the protection of the material is adopted from the conclusions drawn from the simulated test carried out for the purpose. Investigations and studies provide an insight into the mechanisms of material removal during the wear process of the material.[7,8] There are a number of methods to evaluate the erosion wear of materials using equipment, such as small feed rate erosion test equipment,[9] particle jet erosion test equipment,[10] coriolis erosion tester[11] and slinger erosion test equipment.[12] In this study, the solid-particle erosion behaviour of solutionised, artificially aged and annealed condition of AA2014 aluminium alloy has been investigated and compared to each other. The samples were eroded in specially designed solid-particle erosion test equipment. The equipment was designed using ideas presented for different test conditions and materials in the literature.[9–12] In performing the experiments, the particle-impingement angle, the velocity and the pressure were kept constant and different heat-treated samples were eroded in same test conditions for the test equipment. Furthermore, aluminium alloys exhibit ductile erosion behaviour by showing maximum erosion rates at acute angles (15°–45°). Hence, a 45° impingement angle was used in order to erode the samples effectively. The 75 m/s impingement velocity with 3 bar gas pressure was selected for the optimum erosion of ductile materials by using 180-mesh garnet erodent particles.[5–7,9–12] Increasing the velocity may cause the breaking of the garnet erodent particles owing to impacting on the metal surfaces. The test set up has versatile properties and all the parameters are also changeable with the special mechanisms to perform different test conditions. The microstructures of the solutionised, artificially aged and annealed AA2014 specimens were obtained using a light microscope and an SEM. Moreover, the erosion rates of the samples versus the thermal treatment grades of the AA2014 were calculated and the surface morphologies of the samples were presented by interpreting before and after the erosion tests.

2 EXPERIMENTAL

2.1 Material and Applied Heat Treatments

Initially, the diameter 152 mm (6 inch) AA2014 extrusion billet, with the chemical composition presented in **Table 1**, was produced by an industrial vertical air slip DC casting unit and homogenised at 480 °C for 12 h. The billet was subsequently heated to 430 °C and extruded into a diameter bar 100 mm.

Table 1: The chemical composition of the alloy AA2014 for particle erosion tests in mass fractions, *w*/%

Tabela 1: Kemijska sestava zlitine AA2014 za preizkus erozije z delci v masnih deležih, *w*/%

Al	Si	Fe	Cu	Mn	Mg	Zn	Cr	Ti	Pb
92.92	0.35	0.56	4.56	1.06	0.28	>0.15	0.01	0.02	0.01

Samples from a square cross-section of AA2014 alloy from the extruded bar were cut out (transverse section of extruded bar) with a size of 40 mm × 40 mm × 3 mm. The samples were divided into three separate groups. The first group was soaked at 570 °C for 2 h to achieve the solution heat-treated state and water quenched. The second group was additionally soaked at 160 °C for 12 h to achieve T6 precipitation. Finally, the last group, after T6, was soaked at 410 °C for 3 h to achieve annealing. All the heat treatments were carried on in an electronically operated Severn heat-treating furnace.

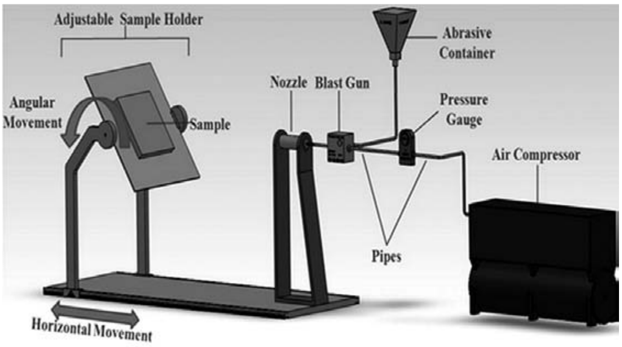

Figure 1: Solid particle erosion test equipment

Slika 1: Naprava za preizkušanje erozije s trdnimi delci

2.2 Erosion test

The erosion tests were performed in a horizontal sand-blast type erosion test equipment. **Figure 1** shows a schematic illustration of the erosion test equipment. Garnet particles with a size of 180-mesh driven by a static air pressure of 3 bar were accelerated along a nozzle 50 mm of diameter 5 mm. The velocity of the particles under 3 bar pressure was 75 m/s measured using the double-disc method. All the erosion experiments were run at a 75 m/s particle-impingement velocity and a 45° angle of impingement (angle of highest wear rates achieved) by using 180-mesh garnet particles. The samples were cleaned with air blasting before and after the erosion tests in order to remove the sand and dust particles, and then the samples were weighed in an electronic balance with an accuracy of ± 0.1 mg.

2.3 Hardness

The hardness of heat-treated samples was measured with a Shimazdu HMV Vickers hardness setup. The test load 300 g and the dwell time 20 s were applied and reported as the average of a minimum 5 readings (HV 0.3). The hardness results were evaluated by generating the hardness graph versus the mass loss.

2.4 Scanning electron microscope

To characterize the morphology of the eroded surfaces and in order to understand the material-removal mechanism, the eroded surfaces of the samples were

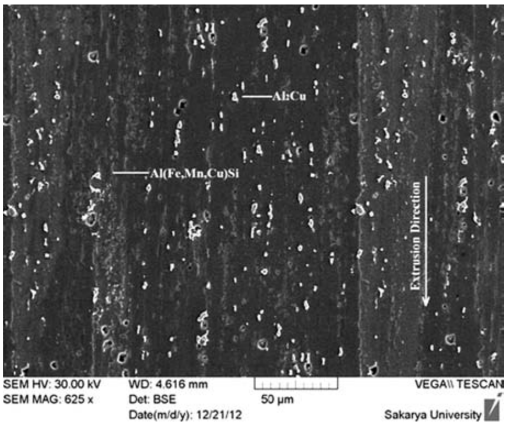

Figure 2: SEM image of longitudinal section of hot-extruded AA2014
Slika 2: SEM-posnetek vzdolžnega prereza vroče ekstrudiranega AA2014

examined using a scanning electron microscope Tescan Vega Sbu–II (Bruker EDS).

3 RESULTS AND DISCUSSION

3.1 Microstructure

Elongated α-Al grains and intermetallic precipitates were settled in the hot-extruded AA2014 bar (**Figure 2**). In the analysis of the structure by SEM, two different types of intermetallic particles with different contrasts were observed at the α-Al grain borders. These are the light- and dark-gray intermetallic particles. The EDS analysis of the light-gray particles reveals a reflection of the Al and Cu signals. However, dark-grey particles additionally reflected the Si, Mn and Fe signals. According to the XRD spectrum, the light- and dark-grey particles are the soluble Al_2Cu and the insoluble cubic α_c-Al_{12}(Fe, Mn, Cu)$_3$Si, respectively, as seen in **Figure 3**. The lack of evidence for recrystallisation across the section of the hot-extruded bar implies that the deformation introduced during the extrusion process is restricted by the pinning effect of the Al_2Cu.

According to the EDS analysis (**Figures 4b** to **6b**) of the grain boundaries of the solutionised sample, it was clearly detected that there was no response of the Al_2Cu signals. Heating the samples at 570 °C for 2 h resulted in a fully solutionised structure and the dissolution of the soluble eutectic Al_2Cu into the matrix. Also, the remaining of intermetallics verify the insolubility of α_c-Al_{12}(Fe,

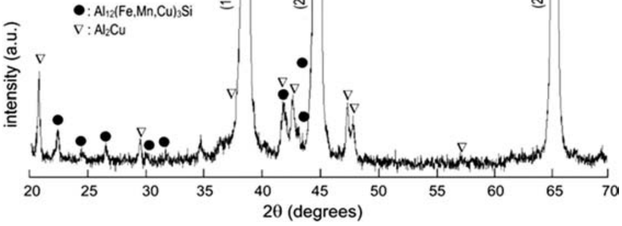

Figure 3: XRD spectrum of as-received AA2014
Slika 3: XRD-spekter dobavljenega AA2014

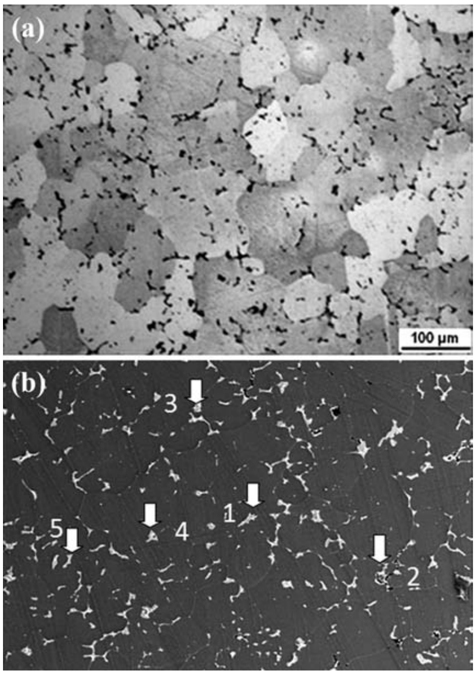

Point 1: Al 58.8, Cu 20.0, C 11.2, Mn 5.2, Fe 4.7, **Point 2:** Al 72.8, Cu 11.7, Mn 6.8, Fe 5.6, Si 3.1, **Point 3:** Al 59.5, C 28.8, Cu 8.0, Si 3.6, **Point 4:** Al 90.1, Cu 8.0, Mn 1.9, **Point 5:** Al 51.4, C 43.6, Cu 5.0 (mass fractions, *w*/%)

Figure 4: a) Light-microscope view of the solution heat-treated sample, b) indicated points of EDS analysis of solution heat-treated sample
Slika 4: a) Mikrostruktura raztopno žarjenega vzorca, b) označena mesta EDS-analiz raztopno žarjenega vzorca

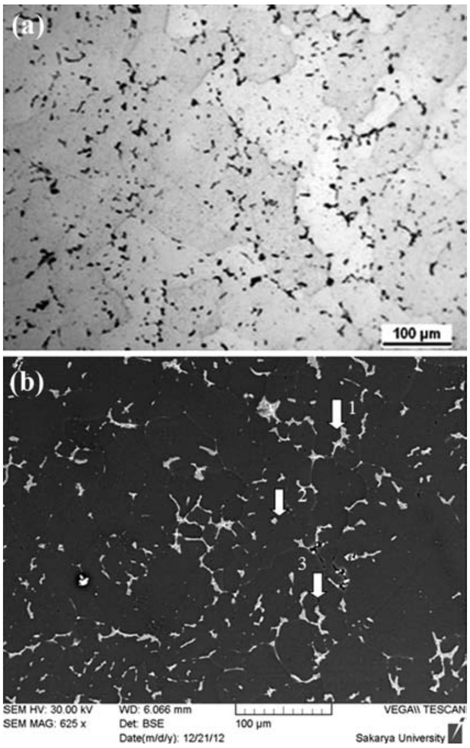

Point 1: Al 58.5, Cu 31.8, C 8.9, Si 0.8; **Point 2:** Al 62.0, Cu 38.0; **Point 3:** Al 56.1, Cu 3.9 (mass fractions, *w*/%)

Figure 5: a) Light-microscope view of T6 sample, b) indicated points of EDS analysis of T6 treated sample
Slika 5: a) Mikrostruktura vzorca po T6 toplotni obdelavi, b) označena mesta EDS-analiz vzorca po T6 toplotni obdelavi

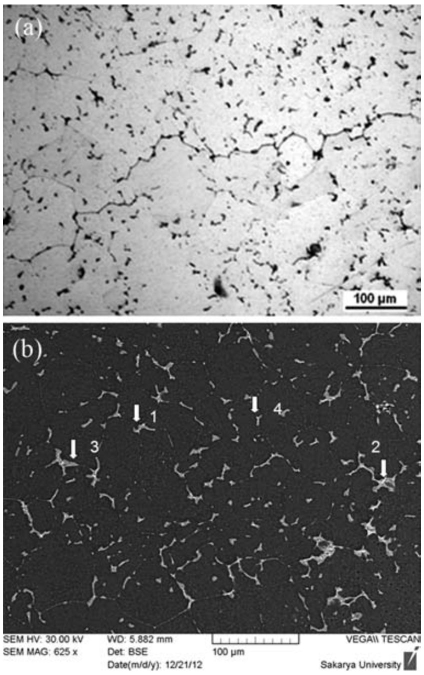

Point 1: Al 80.6, Cu 15.7, Si 3.7; **Point 2:** Al 47.8, Cu 19.2, Mn 11.5, Fe 9.8, Si 1.0; **Point 3:** Al 71.5, C 16.9, Mn 5.1, Fe 3.5, Si 2.9; **Point 4:** Al 85.5, C 10.0, Cu 4.5 (mass fractions, *w*/%)

Figure 6: a) Light-microscope view of annealed sample, b) indicated points of EDS analysis of annealed sample

Slika 6: a) Mikrostruktura mehko žarjenega vzorca, b) označena mesta EDS-analiz mehko žarjenega vzorca

Mn, Cu)$_3$Si. A light-microscope view of the solutionised sample was presented in **Figure 4a**.

Holding the sample at an elevated temperature assists in the segregation of the Si from the matrix to the grain boundary. Thus, the chemical composition of the grain boundary becomes closer to the Al-Si-Cu ternary eutectic. Also, it forces the grains to coarsen. Especially during the annealing stage, the precipitates, which occurred for T6 indicated in **Figure 5a**, start to coarsen and settle on the grain boundary, also become detectable by EDS analysis, as seen in the **Figure 6b**. A light-microscope view of the annealed sample is presented in **Figure 6a**.

3.2 Erosion rate

Samples prepared under three different heat-treatment conditions were exposed to erosive wear in the test equipment demonstrated in **Figure 1** with the parameters explained in **Table 2**. The results from the experiments are showed in **Table 2**. The code numbers indicated in the first column of **Table 2** define the surfaces of the samples exposed to different heat-treatment conditions. K1$_f$ means the front surface of the square cross-section for the sample prepared by the solution treated AA2014. Similarly, K1$_b$ means the back side of the solution-treated sample of AA2014. The code numbers of K2$_f$ and K2$_b$ mean the front side and back side of the samples prepared from the AA2014 extrusion under T6 conditions. The third sample, coded as K3$_f$, K3$_b$, means the front and back sides of the samples prepared from AA2014 under the annealed condition of the samples after the T6 precipitation hardening. Furthermore, to analyze the erosion rates and the hardness of samples on the different heat-treated AA2014 by keeping a constant erosion time, the impingement angle and air pressure, a graphical representation was indicated in **Figure 7**.

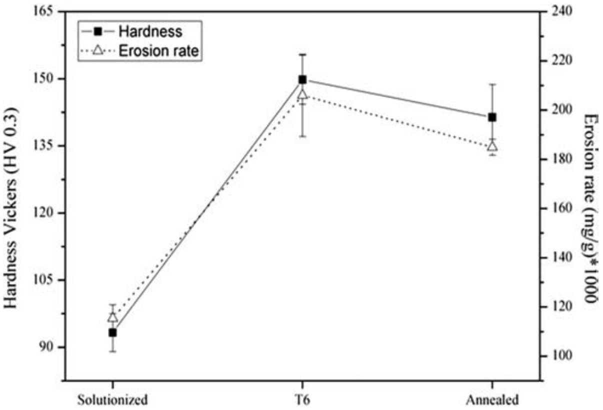

Figure 7: Erosion rates and hardness of solution heat treated, heat treated and annealed AA2014

Slika 7: Hitrosti erozije in trdote raztopno žarjenega, toplotno obdelanega in mehko žarjenega AA2014

3.3 Interpretation on Surface Morphology of the Eroded Samples

In this section, the idea was to examine and understand the effects of the heat-treatment conditions on the surface morphology of the samples before and after the erosion tests. Moreover, the aim was to detect and discuss the dominant erosion mechanisms. Hence, in **Figures 8** to **10**, SEM image studies of the surfaces of

Table 2: Erosive test parameters applied to the AA2014 and the measured results

Tabela 2: Parametri preizkusa erozije na AA2014 in izmerjeni rezultati

Sample Code	Constant parameters applied to testing of each samples	Initial mass m_1/g	Final mass m_2/g	Δm/mg	Δm (mean)/ 1000 mg	Erosion rate (mg/g) ×1000
K1$_f$	Erosion time (s): 20 Impingement Angle (°): 45 Pressure (bar): 3 Mesh: 180 Mass volume (g/s): 6.76	35.81	35.79	16.70	15.60	115.38
K1$_b$		35.79	35.78	14.50		
K2$_f$		34.70	34.67	25.30	27.85	205.99
K2$_b$		34.67	34.64	30.40		
K3$_f$		35.54	35.52	25.00	25.00	184.91
K3$_b$		35.52	35.49	25.00		

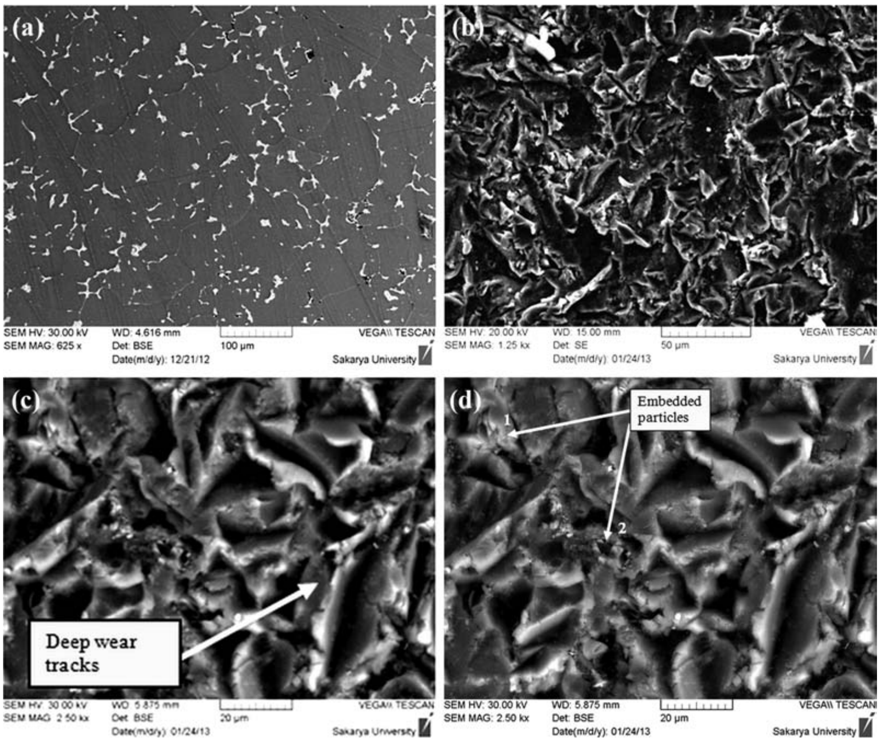

Figure 8: SEM images of solution heat treated AA2014 samples: a) surface before erosion (SE mode), b) eroded surface (SE mode), c) eroded surface (BSE mode), d) indicated points of EDS analysis of the solutionised and eroded sample

Slika 8: SEM-posnetki raztopno žarjenih vzorcev AA2014: a) površina pred erozijo (način SE), b) erodirana površina (način SE), c) erodirana površina (način BSE), d) označena mesta EDS-analiz raztopno žarjenega in erodiranega vzorca

the solutionised, annealed and heat-treated samples were performed. The SEM images of the samples were taken before and after the erosion process and were taken in the SE (secondary electron) and BSE (back scattered electron) modes in the SEM. Furthermore, an EDS analysis of the eroded surfaces of the samples were taken along with the SEM investigations and were given in this section. In **Figures 8a** to **8d**, SEM images and EDS results of the solutionised alloy were given. The micro-cutting and the micro-ploughing erosion mechanisms can be seen in **Figures 8b** to **8d**.

The erosion of the surface of the samples caused by the impact of the erodent particles can be seen by comparing **Figures 8b**, **9b** and **10b**. Although the solutionised aluminium AA2014 has low erosion rates, as indicated in **Figure 7**, the surfaces of the samples after exposing to solid particle erosion were also damaged significantly. In **Figure 8d** an EDS analysis of the surfaces of the solutionised aluminium alloy were given. The existence of the O and Fe atoms in a high percentage was the evidence for the embedded erodent garnet particles to the surfaces of the samples. Based upon the EDS analysis results, it was concluded that the erodent particles were embedded in the surfaces of the aluminium alloy during the erosion process.

Moreover, it was also concluded that this could be possible because of the ductile behaviour of the aluminium alloy. In the literature[7,12] of solid particle erosion, most metals undergo erosion by ductile erosion behaviour and the erodent particles with high velocities can be embedded to the surfaces of the samples specifically at obtuse impingement angles, such as 75° and 90°. However, in this study the samples were eroded at 45° impingement angles and it was not expected to detect the embedded erodent particles. The embedded particles on the surfaces of the solutionised aluminium alloy were clearly observed in SEM studies. Thus, it can be concluded that erodent particles can also be embedded in the surfaces of the aluminium alloys at acute impingement angles, which have not been mentioned in the literature before. In **Figures 9a** to **9d**, the SEM images and EDS results of the artificially aged T6 AA2014 alloy were given. The micro-cutting and the micro-ploughing erosion mechanisms can be seen in **Figures 9b** to **9d**.

Hence, it can be concluded that the solid particle erosion causes significant damage on the surfaces of the artificially aged (T6) aluminium alloy. The low plastic deformation and the shallow depth of the craters and lips can be observed on the specimens of T6-treated AA2014. In **Figure 9d** an EDS analysis of the surface of the T6 treated AA2014 specimen was given. Similarly, the existence of the O and Fe atoms in a high percentage was the evidence of the embedded erodent garnet particles to the surfaces of the samples. Based upon the EDS analysis results, it was concluded that the erodent particles were embedded in the surfaces of the aluminium

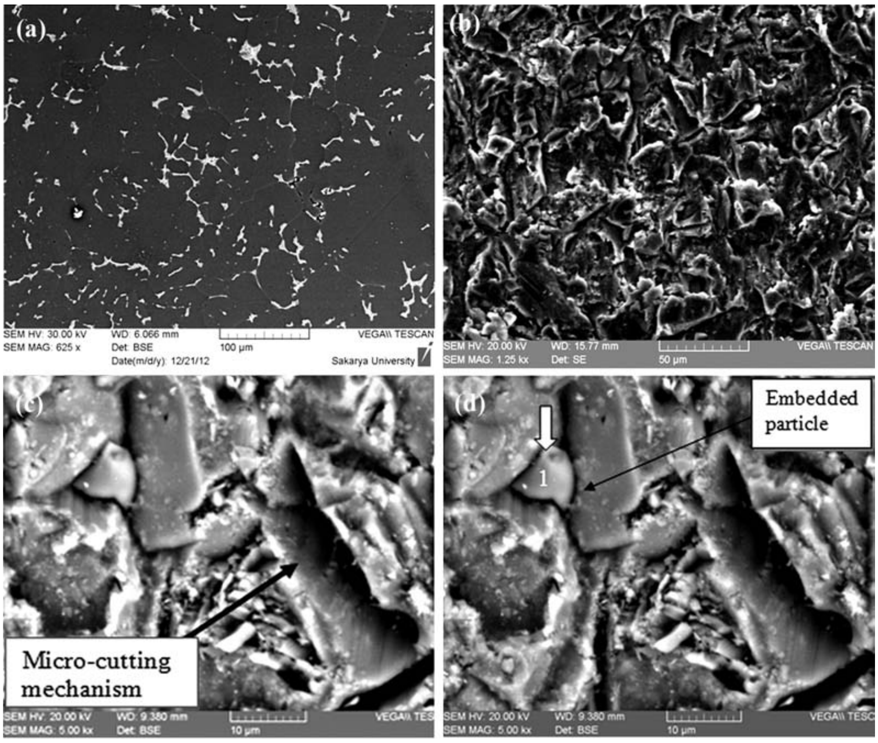

Point 1: O 33.1, Fe 25.5, Si 18.1, Al 14.7, Mg 6.8, Ca 1.3, C 0.6 (mass fractions, *w*/%)

Figure 9: SEM images of artificially aged (T6) AA2014 samples: a) surface before erosion (SE mode), b) eroded surface (SE mode), c) eroded surface (BSE mode), d) indicated point of EDS analysis of artificially aged (T6) sample

Slika 9: SEM-posnetki umetno staranih (T6) AA2014 vzorcev: a) površina pred erozijo (način SE), b) erodirana površina (način SE), c) erodirana površina (način BSE), d) označeno mesto EDS-analize umetno staranega vzorca

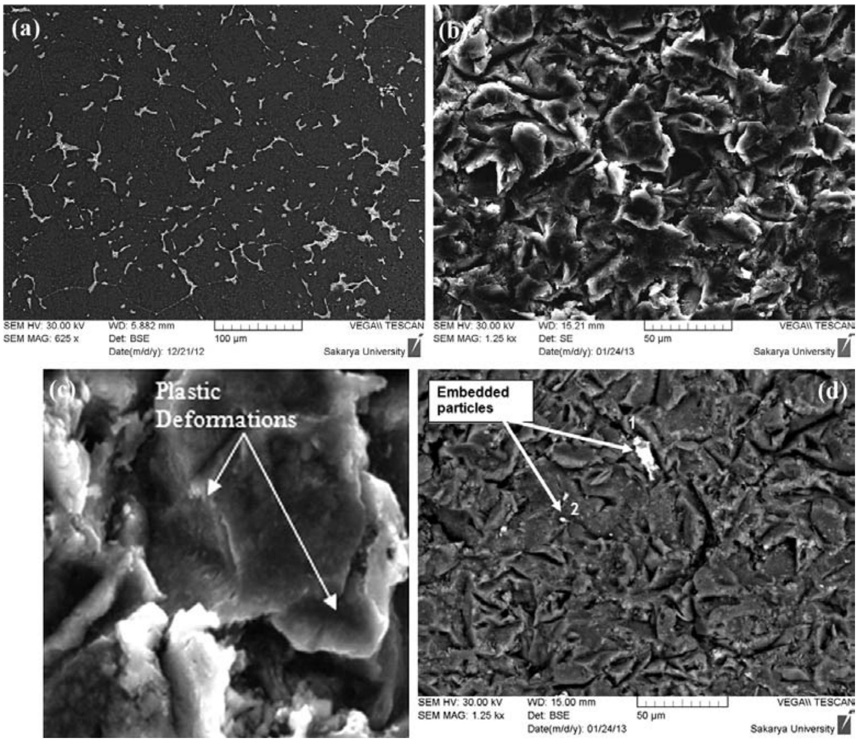

Point 1: Fe 75.0, N 19.4, Al 4.8, Si 0.4; **Point 2:** Al 47.4, O 30.7, Ca 11.5, C 4.0, Cu 2.2, Si 1.6, Fe 1.6, Mg 1.2 (mass fractions, *w*/%)

Figure 10: SEM images of annealed AA2014 samples: a) surface before erosion (SE mode), b) eroded surface (SE mode), c) eroded surface (BSE mode), d) indicated points of EDS analysis of the annealed sample

Slika 10: SEM-posnetki mehko žarjenih AA2014 vzorcev: a) površina pred erozijo (način SE), b) erodirana površina (način SE), c) erodirana površina (način BSE), d) označena mesta EDS-analiz mehko žarjenega vzorca alloy during the erosion process. However, in this study the samples were eroded at 45° impingement angles and it was not expected to detect embedded erodent particles. The embedded particles on the surfaces of the aluminium alloy AA2014 applied artificial aging seen on the **Figure 9d** were clearly seen in the SEM studies. Hence, it can be concluded that the erodent particles can also be embedded in the surfaces of the aluminium alloys at acute impingement angles (45°), which have not been mentioned in the literature before.

In **Figures 10a** to **10d** the SEM images and EDS results of the annealed AA2014 alloy are given. The micro-cutting and the micro-ploughing erosion mechanisms can be seen in **Figures 10b** to **10d**. Hence, it can be concluded that solid particle erosion causes significant damage on the surfaces of the annealed aluminium alloy. The depth of the craters created by the blocking of the kinetic energy of the accelerated particles is lower than the solutionised structure.

The flake formation and work-hardened layer are generated when the surface suffers extensive plastic deformation. The impacts of solid particles break the flake and the outer work-hardened layer. Thus particles cause the erosive loss of the material. In **Figure 10d** an EDS analysis of the surfaces of the annealed aluminium alloy is given. The existence of the O and Fe atoms in high percentages was the evidence of the embedded erodent garnet particles to the surfaces of the samples. Based upon the EDS analysis results, it was concluded that the erodent particles were embedded in the surfaces of the aluminium alloy during the erosion process. Annealed AA2014 has a ductility higher than AA2014 T6, so that the material erosion rate is lower. This means that if the machine parts designed with light metals are exposed to particle erosion owing to functionality of the process, they should be used in ductile conditions in the construction rather than the T6 artificial aging hardening state.

4 CONCLUSION

The alloy AA2014 was exposed to erosive wear by keeping constant the variables such as attack angle, air pressure, particle mass flow and changing ductility conditions of the material. From the studied parameters, the results can be summarized as:

- Experiments indicated that the erosive wear of the aluminium AA2014 increases with increasing hardness of the material. Increasing of the material hardness caused increasing of the brittleness and decreasing ductility. Thus, the kinetic energy of the moving particles takes the chip easily from the brittle surface of the AA2014, so that the loss of the material occurs at higher rates from the metal matrix exposed to precipitated hardness.
- To obviate a higher metal-removal rate against excessive particle impingements, material AA2014 should be used under low hardness conditions. The total kinetic energy of the erodent is exhausted in the crater formation. Due to the large difference in the hardness of the erodent and the specimen surface, a crater would be easily created on the surface.
- Wear mechanisms at the different rated surfaces take place by cutting, impingement and removal of the material from the surface of the specimen. Furthermore, embedded erodent particles were observed on the surfaces of the solutionised, heat-treated and annealed specimens of aluminium AA2014. It was concluded that the erodent particles can also be embedded in the surfaces of the aluminium alloys at acute impingement angles due to the ductility of the samples.

5 REFERENCES

[1] Y. I. Oka, K. Okamura, T. Yoshida, Practical Estimation of Erosion Damage Caused by Solid Particle Impact Part 1: Effects of Impact Parameters on A Predictive Equation, Wear, 259 (**2005**), 95–101

[2] A. R. Harne, Life Improvement of Thermal Power Station Component: A War Against Wear Workshop on Wear and Erosion of Materials in Thermal Power Station, CPRI, Bangalore, 1989

[3] B. Yücel, E. A. Güven, L. Çapan, Extrusion of EN AW-2014 Alloy in Semisolid state, Materials Science and Technology, 27 (**2011**), 1851–1857

[4] B. K. Prasad, S. Das, A. K. Jha, O. P. Modi, R. Dasgupta, A. H. Yegneswaran, Factors Controlling the Abrasive Wear Response of a Zinc-Based Alloy Silicon Carbide Particle Composite, Composites A, 28 (**1997**), 301–308

[5] A. K. Jha, A. Gachake, B. K. Prasad, R. Dasgupata, A. H. Yegneswaran, High Stress Abrasive Wear Behavior of Some Hard Faced Surfaces Produced by Thermal Spray, Journal of Materials Engineering and Performance, 11 (**2002**) 1, 37–45

[6] K. Sanjay, D. P. Mondal, A. K. Jha, Effect of Microstructure And Chemical Composition of Hard Facing Alloy on Abrasive Wear Behavior, Journal of Materials Engineering and Performance, 9 (**2002**) 6, 649–655

[7] I. Finnie, K. Natesan, The mechanism of erosion wear in ductile material: Corrosion behavior of materials [J]. TMS-AIME, (1980), 118–126

[8] T. Denga, M. S. Bingleya, M. S. A. Bradleya, S. R. De Silva, A Comparison of The Gas-Blast and Centrifugal-Accelerator Erosion Testers: The Influence of Particle Dynamics; Wear, 265 (**2008**), 945–955

[9] W. Zhu, Z. Y. Mao, Wear of Material [C]// LUDEMA K C ed. Proceeding of Conference Wear of Material, ASME, 787, 1987

[10] R. G. Desale, K. Bhupendra, S. C. Gandhi, Improvement In the Design of a Pot Tester to Simulate Erosion Wear due to Solid-Liquid Mixture, Wear, 259 (**2005**), 196–202

[11] H. M. H. Throhe, Y. Xie, S. K. Yick, A New Coriolis Slurry Erosion Tester Design for Improved Slurry Dynamics, Wear, 255 (**2003**), 170–180

[12] T. Denga, M. S. Bingley, M. S. A. Bradley, Understanding Particle Dynamics in Erosion Testers – A Review of Influences of Particle Movement On Erosion Test Conditions, Wear, 267 (**2009**), 2132–2140